Electronic Supplementary Material (ESI) for Photochemical & Photobiological Sciences.

Supporting Information for

One- and two-photon absorption properties of quadrupolar thiophene-based dyes with acceptors of varying strength

Sofia Canola,[a,b] Lorenzo Mardegan[a], Giacomo Bergamini[a], Marco Villa[a], Angela Acocella[a], Mattia Zangoli[c], Luca Ravotto[d], Sergei A. Vinogradov[d,*], Francesca Di Maria[e,*], Paola Ceroni[a,*], Fabrizia Negri [a,b,*]

[a] Università di Bologna, Dipartimento di Chimica 'G. Ciamician', Via F. Selmi, 2, 40126 Bologna, Italy

[b] INSTM, UdR Bologna, Italy.

[c] MEDITEKNOLOGY srl, Via P. Gobetti 101, 40129 Bologna Italy

[d] University of Pennsylvania, Department of Biochemistry and Biophysics, Perelman School of Medicine, Philadelphia, PA 19104, USA

[e] CNR-NANOTEC - Istituto di Nanotecnologia, Via Monteroni, 73100 Lecce, Italy.

^{1}H AND ^{13}C NMR SPECTRA

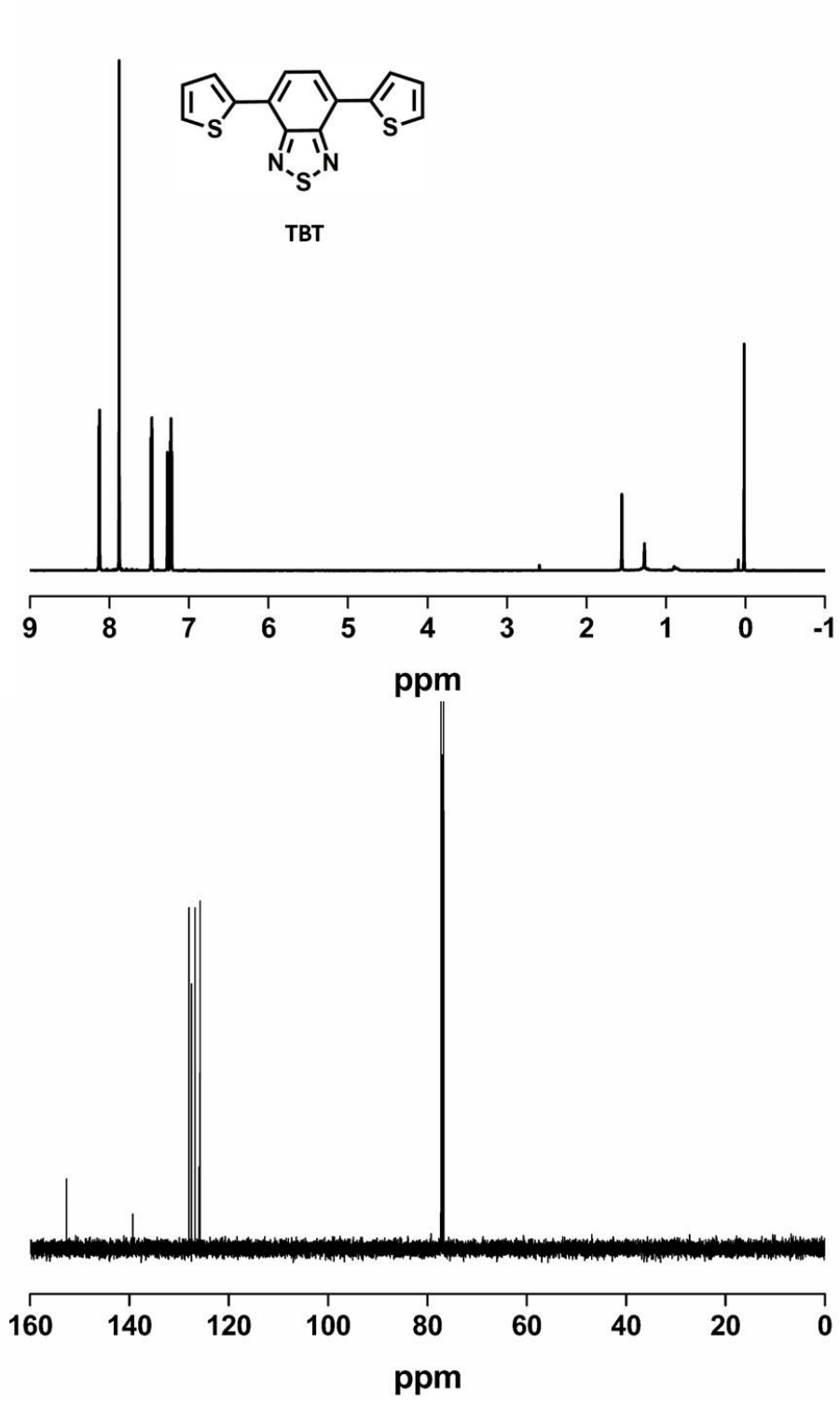

^{1}H and ^{13}C NMR spectra of TBT in $CDCl_3$

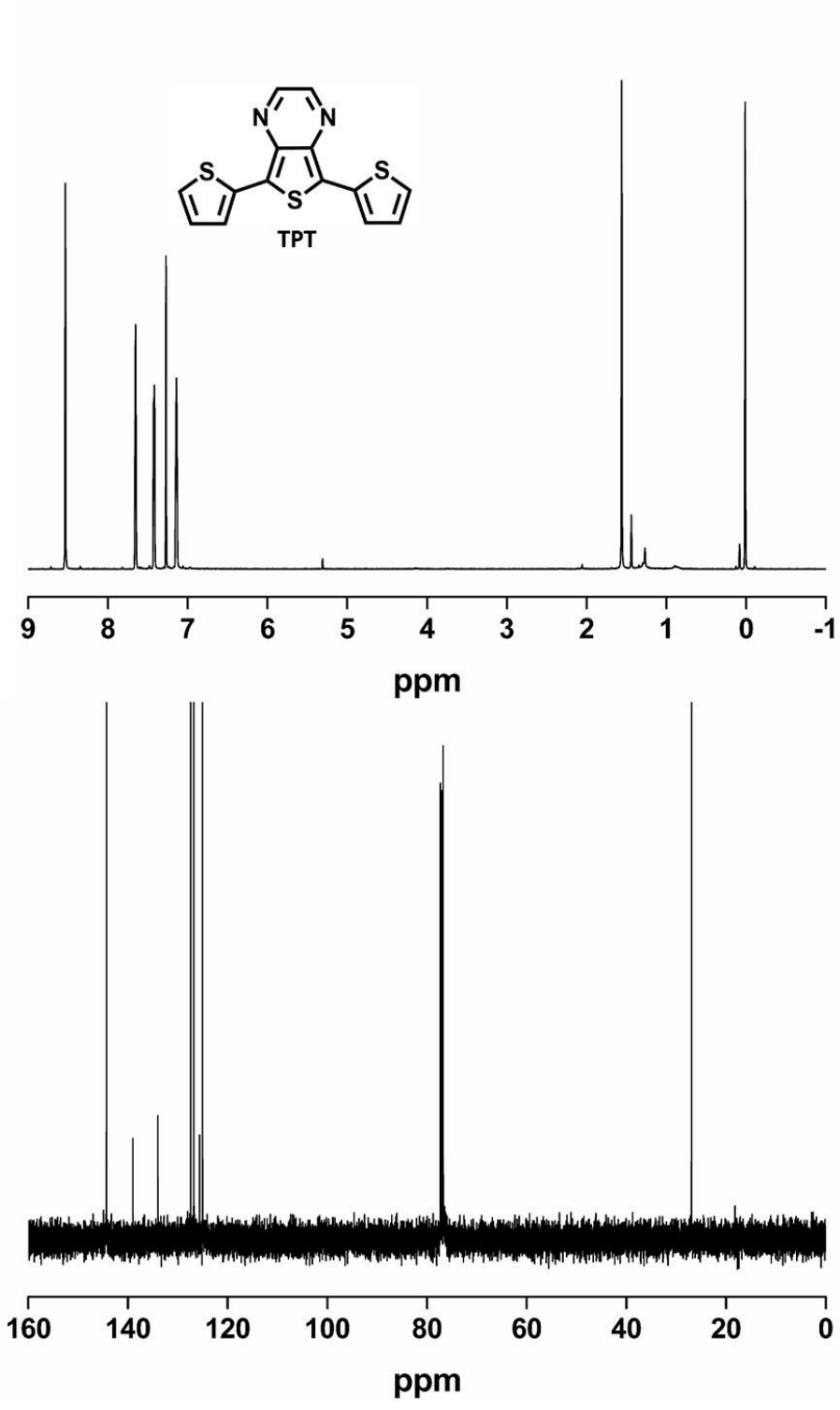

^{1}H and ^{13}C NMR spectra of TPT in $CDCl_3$

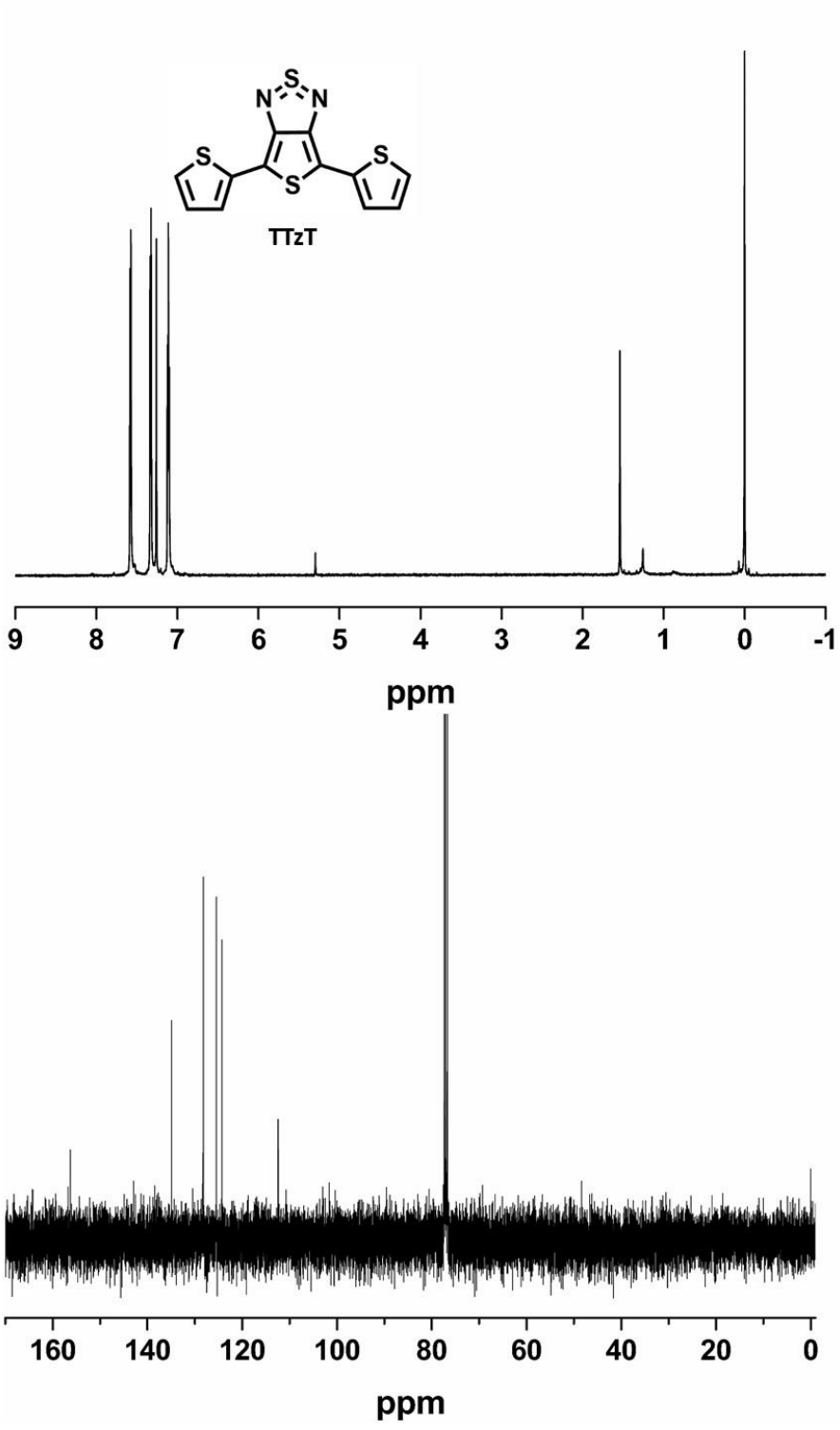

^{1}H and ^{13}C NMR spectra of TTzT in $CDCl_3$

Vibronic structure simulation.

The evaluation of the Franck-Condon (FC) vibronic progressions in electronic spectra [1-3] requires the evaluation of the Huang–Rhys (HR) factors S_v [4,5], for each vibrational mode *v* with frequency ω_v. S_v is obtained from the dimensionless displacement parameters B_v, assuming the harmonic approximation and neglecting Duschinski[6] rotation:

$$B_v = \sqrt{\frac{\omega_v}{\hbar}}\left[\boldsymbol{X_j} - \boldsymbol{X_i}\right]\boldsymbol{M}^{1/2}\boldsymbol{Q}_v(j) \tag{S1}$$

and hence defined as

$$S_v = \frac{1}{2}{B_v}^2 \tag{S2}$$

where $\boldsymbol{X}_{i,j}$ is the *3N* dimensional vector of the equilibrium Cartesian coordinates of the *i,j* electronic state (here the ground and excited molecular states), $\boldsymbol{M}$ is the *3N×3N* diagonal matrix of atomic masses and $\boldsymbol{Q}_v(j)$ is the *3N* dimensional vector describing the *v* normal coordinate of the *j* state in terms of mass weighted Cartesian coordinates.

From preliminary calculations carried out in vacuo it was verified that frequency changes upon excitation are not relevant and that a mirror image is retained between the absorption and emission vibronic structures. For this reason and because of the number of solvents investigated, vibronic progressions were simulated always using ground state frequencies. While this approach is approximate, and less rigorous than that discussed in recent work[7-15], it is justified by the minor changes upon excitation, computed for the active frequencies.

For each normal mode *v*, the Franck-Condon factor *FC* for a transition from a vibrational level *m* (of the electronic state *i*) to the vibrational level *n* (of the electronic state *j*) is [16]:

$$FC_v(m,n)^2 = e^{-S_v}{S_v}^{n-m}\frac{m!}{n!}\left(L_m^{(n-m)}(S_v)\right)^2 \tag{S3}$$

where *L* is a Laguerre polynomial. The intensity $I_v(m,n)$ of the *m* to *n* transition for the normal mode *v* is the *FC* factor, weighted for the population of the *m* vibrational state:

$$I_v(m,n) = FC_v(m,n)^2\,\frac{\exp(\frac{-m\hbar\omega_v}{k_BT})}{Z} \tag{S4}$$

with k_B the Boltzmann constant, T the temperature and Z the partition function. The total intensity of the multimode vibrational transition, including all the active normal modes, is the simple product of the monodimensional intensities [17].

Absorption and emission spectra were simulated at T=300K. A Gaussian broadening function, hwhm=0.4 eV was superimposed to each computed intensity.

Table S1. Ground and lowest excited state dipole moment (Debye) of **TBT**, **TPT** and **TTzT** from CAM-B3LYP/6-31G* level of theory in vacuo and solvent described with the PCM model.

	$\mu[S_0(tt)]$	$\mu[S_0(cc)]$	$\mu[S_1(tt)]$	$\mu[S_1(cc)]$
			TBT	
Vacuo	0.0281	2.1689	3.3994	5.3437
CHex	0.0429	2.5552	3.6654	5.6411
$CHCl_3$	0.0783	2.9287	3.9021	6.2303
THF	0.0962	3.0394	3.9885	6.4540
DCM	0.1023	3.1203	4.0162	6.5240
EtOH	0.1267	3.2513	4.1135	6.7788
ACN	0.1309	3.3183	4.1316	6.8246
DMF	0.1316	3.2855	4.1333	6.8308
DMSO	0.1336	3.3362	4.1417	6.8511
			TPT[a]	
Vacuo	0.4903	1.4078	3.3984	1.9335
CHex	0.6065	1.6082	3.7537	1.9739
$CHCl_3$	0.7654	1.7690	4.0965	1.9672
THF	0.8342	1.8214	4.2261	1.9578
DCM	0.8578	1.8375	4.2683	1.9542
EtOH	0.9450	1.8905	4.4176	1.9317
ACN	0.9630	1.8998	4.4436	1.9284
DMF	0.9647	1.9007	4.4463	1.9281
DMSO	0.9726	1.9049	4.4594	1.9266
			TTzT	
Vacuo	1.9903	0.0196	4.9552	3.3138
CHex	2.2952	0.0314	5.5820	3.6374
$CHCl_3$	2.6137	0.0330	6.1568	3.8905
THF	2.7379	0.0295	6.3664	3.9734
DCM	2.7785	0.0280	6.4338	3.9991
EtOH	2.9232	0.0209	6.6682	4.0849
ACN	2.9505	0.0193	6.7118	4.1003
DMF	2.9532	0.0192	6.7160	4.1018
DMSO	2.9658	0.0184	6.7361	4.1088

[a] Note that for the *cc* conformer of **TPT** the ground and excited dipole moment has similar magnitude but opposite direction.

Table S2. Lowest four excited states of **TBT**, **TPT** and **TTzT** computed in vacuo at TD-CAM-B3LYP/6-31G* level of theory: excitation energies (*Exc*), oscillator strength (*f*), wavefunction (*wf*, indicating coefficients and orbitals involved in the excitation).

	Exc / eV	*Exc / nm*	*f*	*wf.*	
			tt-TBT		
S1	2.97	418	0.429	H→L	0.70
S2	4.40	282	0.040	H-1→L	0.62
S3	4.52	274	0.434	H→L+1	0.65
S4	4.53	274	0.045	H-4→L	0.44
				H-2→L	-0.37
S5	4.74	262	0.083	H-3→L	0.65
				H→L+1	-0.21
			tt-TPT		
S1	2.55	486	0.352	H→L	0.70
S2	3.54	350	0.002	H-4→L	0.66
S3	4.20	295	0.424	H→L+1	0.68
S4	4.30	288	0.071	H-5→L	0.31
				H-2→L	0.23
				H-1→L	0.56
S5	4.40	282	0.004	H→L+2	0.39
				H-1→L	-0.38
				H-5→L	0.35
			tt-TTzT		
S1	2.08	597	0.315	H→L	0.70
S2	4.00	310	0.499	H→L+1	0.69
S3	4.04	307	0.049	H-1→L	0.68
S4	4.24	292	0.004	H-2→L	0.66
S5	4.30	288	0.002	H-3→L	0.70

	Exc / eV	*Exc / nm*	*f*	*wf*	
			cc-TBT		
S1	3.04	407	0.438	H→L	0.70
S2	4.38	283	0.009	H-1→L	0.62
S3	4.54	273	0.013	H-2→L	0.50
S4	4.62	268	0.386	H→L+1	0.60
				H-4→L	0.31
S5	4.62	268	0.104	H-4→L	0.50
				H-6→L	-0.29
			cc-TPT		
S1	2.55	486	0.330	H→L	0.70
S2	3.54	351	0.003	H-4→L	0.66
S3	4.14	300	0.407	H→L+1	0.68
S4	4.31	288	0.057	H-2→L	0.42
				H-5→L	-0.36
				H-1→L	-0.32
S5	4.39	282	0.078	H-1→L	0.59
				H→L+2	-0.29
				H-2→L	0.15
			cc-TTzT		
S1	2.07	599	0.296	H→L	0.70
S2	3.93	315	0.463	H →L+1	0.68
S3	4.02	309	0.000	H→L+2	0.69
S4	4.07	305	0.083	H-1→L	0.65
S5	4.27	291	0.006	H-2→L	0.62

Table S3. Frontier orbital energies, *E*(*HOMO*) and *E*(*LUMO*), and their energy gap, *ΔE(H-L)*, of **TBT**, **TPT** and **TTzT** computed at the CAM-B3LYP/6-31G* optimized ground state structures in vacuo and in solvent described with the PCM model.

	E(*HOMO*) / *eV*	*E*(*LUMO*) / *eV*	*ΔE(H-L)* / *eV*	*E*(*HOMO*) / *eV*	*E*(*LUMO*) / *eV*	*ΔE(H-L)* / *eV*
		tt-TBT			**cc-TBT**	
Vacuo	-6.65	-1.50	5.15	-6.66	-1.44	5.23
CHex	-6.68	-1.51	5.17	-6.70	-1.47	5.23
$CHCl_3$	-6.71	-1.53	5.18	-6.73	-1.50	5.24
THF	-6.72	-1.54	5.18	-6.75	-1.50	5.25
DCM	-6.73	-1.55	5.18	-6.75	-1.52	5.24
EtOH	-6.74	-1.56	5.19	-6.78	-1.52	5.25
ACN	-6.75	-1.56	5.19	-6.78	-1.54	5.24
DMF	-6.75	-1.56	5.19	-6.78	-1.53	5.25
DMSO	-6.75	-1.56	5.19	-6.78	-1.54	5.24
		tt-TPT			**cc-TPT**	
Vacuo	-6.24	-1.52	4.73	-6.25	-1.51	4.74
CHex	-6.29	-1.55	4.74	-6.29	-1.54	4.75
$CHCl_3$	-6.34	-1.59	4.75	-6.34	-1.57	4.77
THF	-6.35	-1.60	4.75	-6.36	-1.59	4.77
DCM	-6.36	-1.61	4.75	-6.36	-1.59	4.77
EtOH	-6.38	-1.63	4.75	-6.38	-1.61	4.78
ACN	-6.39	-1.63	4.76	-6.39	-1.61	4.78
DMF	-6.39	-1.63	4.76	-6.39	-1.61	4.78
DMSO	-6.39	-1.63	4.76	-6.39	-1.61	4.78
		tt-TTzT			**cc-TTzT**	
Vacuo	-6.09	-2.00	4.09	-6.10	-1.99	4.11
CHex	-6.12	-2.02	4.10	-6.12	-2.01	4.12
$CHCl_3$	-6.15	-2.05	4.11	-6.15	-2.03	4.13
THF	-6.17	-2.06	4.11	-6.17	-2.04	4.13
DCM	-6.17	-2.06	4.11	-6.17	-2.04	4.13
EtOH	-6.19	-2.07	4.11	-6.19	-2.05	4.14
ACN	-6.19	-2.08	4.11	-6.19	-2.05	4.14
DMF	-6.19	-2.08	4.11	-6.19	-2.05	4.14
DMSO	-6.19	-2.08	4.11	-6.19	-2.05	4.14

Table S4. Experimental (*exp.*) and computed emission energies for the three dyes investigated; the computed emission energies were determined at the excited state geometry with State Specific (*SS*) or Linear response *(LR)* method. Solvent described with PCM model.

	Emiss. SS (eV)	*Emiss. LR (eV)*	*exp. (eV)*
		tt-TBT	
CHex	2.22	2.26	2.31
$CHCl_3$	2.07	2.18	2.13
THF	2.01	2.16	2.18
DCM	1.99	2.15	2.15
EtOH	1.92	2.12	2.11
ACN	1.91	2.12	2.09
DMF	1.91	2.12	2.11
DMSO	1.91	2.11	2.07
		tt-TPT	
CHex	1.83	1.82	1.93
$CHCl_3$	1.69	1.75	1.77
THF	1.70	1.72	1.81
DCM	1.69	1.72	1.78
EtOH	1.65	1.69	1.77
ACN	1.64	1.68	1.78
DMF	1.65	1.68	1.77
DMSO	1.64	1.68	1.76
		tt-TTzT	
CHex	1.46	1.47	1.65
$CHCl_3$	1.33	1.39	1.52
THF	1.28	1.36	1.53
DCM	1.27	1.35	1.50
EtOH	1.21	1.32	1.51
ACN	1.19	1.32	1.49
DMF	1.20	1.32	1.50
DMSO	1.19	1.32	1.46

Table S5. Total calculated Stokes Shift (*Stokes Shift tot.*), along with its vibronic component (*Stokes Shift vibr.*) and electronic component (*Stokes Shift el.*) computed with Linear Response (*Stokes Shift el.-LR*) and State Specific (*Stokes Shift el.-SS)* formalism for the three dyes investigated; calculations carried out with CAM-B3LYP/6-31G* level of theory in vacuo and solvents described with the PCM model. Computed results to be compared with experimental (*exp.*) Stokes Shift.

	Stokes Shift / eV					
	vibr.[a]	*el - SS*	*el - LR*	*tot – SS* [b]	*tot – LR* [c]	*exp.*[d]
			tt-TBT			
CHex	0.488	0.035	-0.001	0.523	0.487	0.467
$CHCl_3$	0.485	0.185	0.069	0.670	0.554	0.650
THF	0.484	0.251	0.101	0.735	0.585	0.601
DCM	0.484	0.266	0.107	0.750	0.591	0.637
EtOH	0.483	0.345	0.143	0.828	0.626	0.665
ACN	0.483	0.361	0.151	0.844	0.634	0.731
DMF	0.483	0.340	0.137	0.823	0.620	0.653
DMSO	0.483	0.349	0.142	0.832	0.625	0.676
			tt-TPT			
CHex	0.483	-0.014	-0.001	0.469	0.482	0.384
$CHCl_3$	0.477	0.077	0.070	0.554	0.547	0.557
THF	0.476	0.121	0.101	0.597	0.577	0.536
DCM	0.476	0.128	0.106	0.604	0.582	0.560
EtOH	0.475	0.182	0.144	0.657	0.619	0.592
ACN	0.476	0.193	0.152	0.669	0.628	0.613
DMF	0.476	0.175	0.138	0.651	0.614	0.589
DMSO	0.476	0.181	0.142	0.657	0.618	0.576
			tt-TTzT			
CHex	0.422	0.010	-0.001	0.432	0.421	0.337
$CHCl_3$	0.423	0.134	0.074	0.557	0.497	0.469
THF	0.425	0.190	0.108	0.615	0.533	0.471
DCM	0.432	0.201	0.113	0.633	0.545	0.502
EtOH	0.431	0.270	0.153	0.701	0.584	0.500
ACN	0.432	0.285	0.161	0.717	0.593	0.544
DMF	0.432	0.265	0.147	0.697	0.579	0.505
DMSO	0.432	0.273	0.152	0.705	0.584	0.541

[a] Estimated from the energy difference between the maxima of absorption and emission simulated spectra (T=300K, gaussian broadening function, hwhm=0.4 eV). [b] Computed as the sum of *vibr.* and *el.-SS* contribution. [c] Computed as the sum of *vibr.* and *el.-LR* contribution. [d] Estimated from the energy difference between the maxima of absorption and emission experimental spectra.

Table S6. Computed optical properties of the first four excited states of **TBT**, **TPT** and **TTzT** (*tt* and *cc* conformers) computed in vacuo at TD CAM-B3LYP/6-31G* level of theory: excitation energies *Exc*, oscillator strength *f* and two photon cross section σ.

		Exc / *eV*	*Exc* / *nm*	*f*	σ / *GM*
tt-TBT					
	S1	2.97	418	0.429	3
	S2	4.40	282	0.040	528
	S3	4.52	274	0.434	20
	S4	4.53	274	0.045	262
	S5	4.74	262	0.083	15
tt-TPT					
	S1	2.55	486	0.352	2
	S2	3.54	350	0.002	0.03
	S3	4.20	295	0.424	78
	S4	4.30	288	0.071	851
	S5	4.40	282	0.004	51
tt-TTzT					
	S1	2.08	597	0.315	3
	S2	4.00	310	0.499	2820
	S3	4.04	307	0.049	$5.27 \cdot 10^5$
	S4	4.24	292	0.004	$1.20 \cdot 10^5$
	S5	4.30	288	0.002	19

		Exc / *eV*	*Exc* / *nm*	*f*	σ / *GM*
cc-TBT					
	S1	3.04	407	0.438	2
	S2	4.38	283	0.009	419
	S3	4.54	273	0.013	232
	S4	4.62	268	0.386	20
	S5	4.62	268	0.104	17
cc-TPT					
	S1	2.55	486	0.330	3
	S2	3.54	351	0.003	0.004
	S3	4.14	300	0.407	72
	S4	4.31	288	0.057	440
	S5	4.39	282	0.078	400
cc-TTzT					
	S1	2.07	599	0.296	3
	S2	3.93	315	0.463	1330
	S3	4.02	309	0.000	0.002
	S4	4.07	305	0.083	$2.47 \cdot 10^6$
	S5	4.27	291	0.006	5260

Table S7. Dipole moments and transition dipole moments (atomic units) components (*x. y. z*) related to the excited states involved in the sum over state (SOS) interpretation of 2P intensities: initial ground state *0*. final state *f* and intermediate state *p=1*.

final state *f*		μ_{00}	μ_{ff}	μ_{0f}^{trs}	μ_{0p}^{trs}	μ_{pf}^{trs}
				tt-TBT		
S2	*x*	0.0000	-0.0002	0.0000	-2.4291	2.5174
	y	-0.0110	0.9283	-0.6067	0.0000	0.0000
	z	0.0009	-0.0014	0.0002	0.0001	-0.0002
S3	*x*	0.0000	-0.0002	-1.9788	-2.4291	0.0004
	y	-0.0110	0.8559	-0.0001	0.0000	1.0048
	z	0.0009	-0.0016	-0.0009	0.0001	-0.0009
S4	*x*	0.0000	0.0002	0.0003	-2.4291	1.4212
	y	-0.0110	0.3820	-0.6342	0.0000	-0.0003
	z	0.0009	-0.0011	0.0011	0.0001	0.0001
				tt-TPT		
S2	*x*	0.0000	0.0000	-0.1599	0.0000	0.0000
	y	0.0000	0.0000	0.0003	2.3726	0.0000
	z	0.1929	0.4253	0.0000	0.0000	0.0002
S3	*x*	0.0000	0.0000	0.0000	0.0000	0.0000
	y	0.0000	-0.0002	-2.0286	2.3726	-0.0004
	z	0.1929	-1.0462	0.0000	0.0000	-1.1613
S4	*x*	0.0000	0.0000	0.0000	0.0000	-0.0001
	y	0.0000	0.0000	0.0000	2.3726	1.6244
	z	0.1929	-0.8804	-0.8197	0.0000	0.0000
				tt-TTzT		
S2	*x*	0.0000	0.0000	0.0000	0.0000	0.0000
	y	0.0000	-0.0002	-2.2566	-2.4910	0.0018
	z	-0.7831	1.4368	0.0000	0.0000	-1.0705
S3	*x*	0.0000	0.0000	0.0000	0.0000	0.0000
	y	0.0000	-0.0002	0.0000	-2.4910	6.1297
	z	-0.7831	1.8591	-0.7044	0.0000	0.0001
S4	*x*	0.0000	0.0000	0.0000	0.0000	0.0001
	y	0.0000	-0.0001	0.0000	-2.4910	2.3210
	z	-0.7831	1.7695	-0.1916	0.0000	0.0000

Table S8. Computed 2P transition probability δ, along with its components δ_F e δ_G, obtained from response theory (RT) and sum over states (SOS) approaches. For the latter two schemes are compared: the first including one intermediate state p ($p=1$) and the second including three intermediate states p (full width half maximum 0.1 eV).

final state f		δ_F (GM)	δ_G (GM)	δ (GM)
tt-TBT				
S2	RT	6070	6260	37200
	SOS($p=1$)	6696	6288	38546
	SOS($p=1,3,4$)	7099	6433	39931
tt-TPT				
S4	RT	10400	10500	62700
	SOS($p=1$)	9947	9170	56572
	SOS($p=1,2,3$)	11138	10311	63519
tt-TTzT				
S2	RT	0.0000	60000	240000
	SOS($p=1$)	0.3434	53917	215668
	SOS($p=1,3,4$)	0.3434	54481	217926

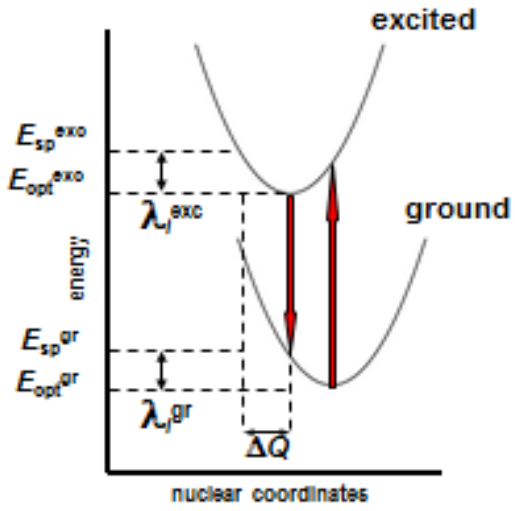

.

Figure S1. Schematic representation of the potential energy curves of ground and excited state of the chromophore and indication of the two contributions to the total internal reorganization energy λ_i. The total reorganization energy is determined as $\lambda_i = \lambda_i^{gr} + \lambda_i^{exc}$

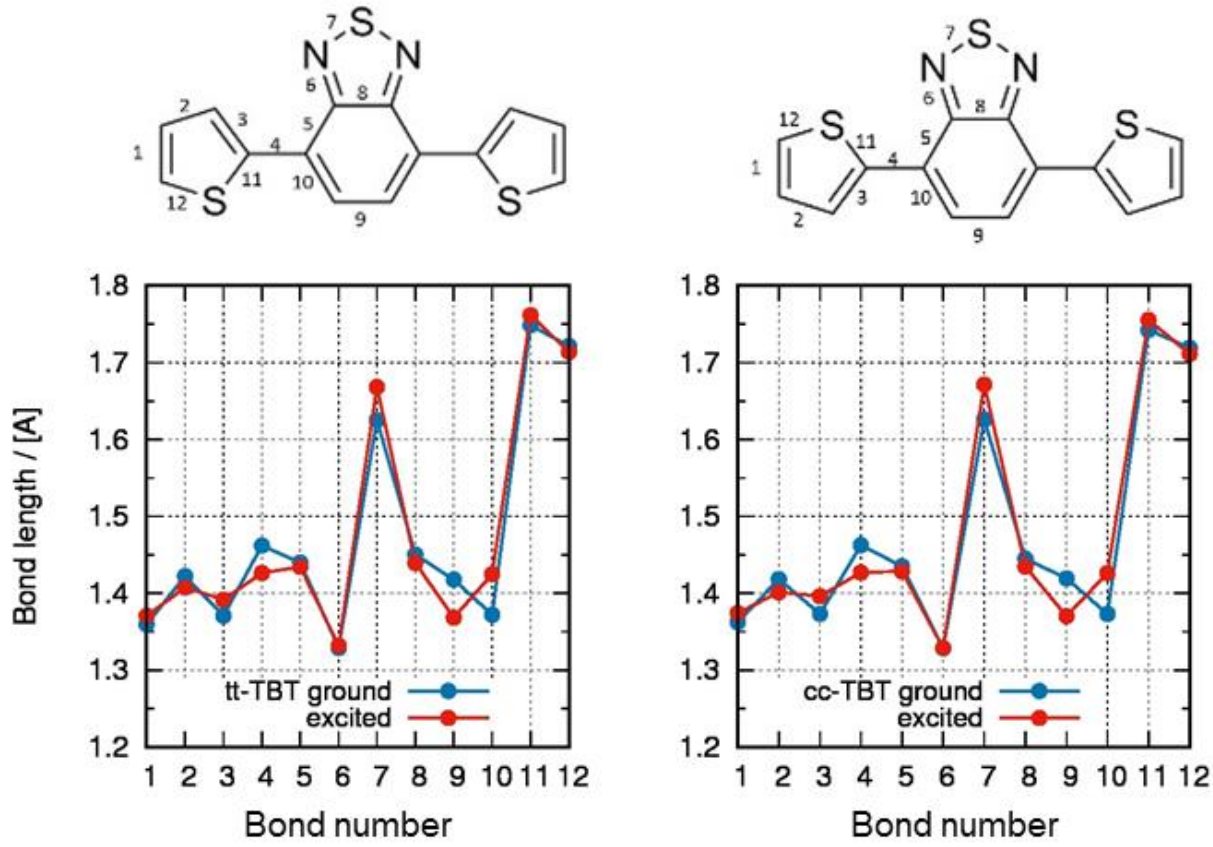

Figure S2. Comparison between the geometry of the ground and lowest excited state of the two conformers of **TBT**, computed at TD-CAM-B3LYP/6-31G* in vacuo.

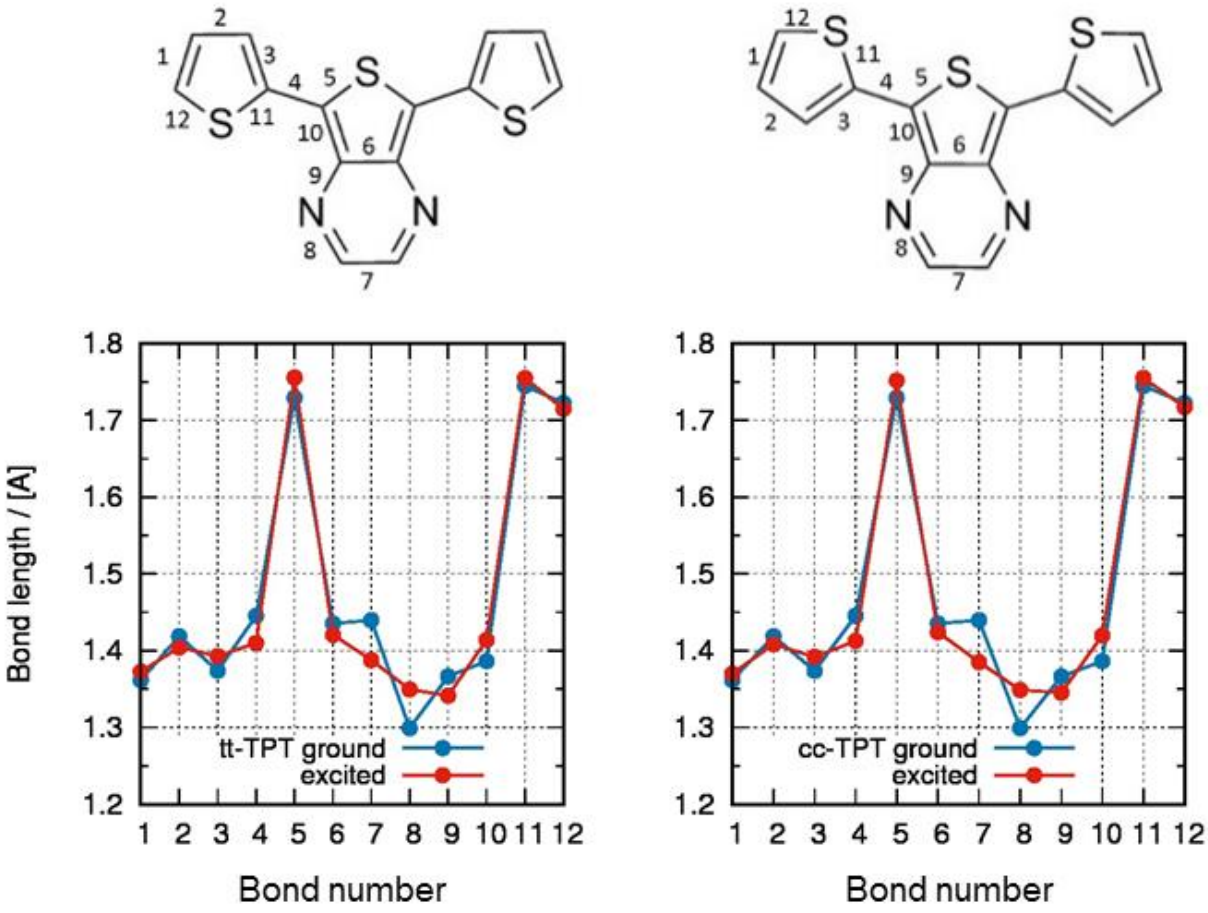

Figure S3. Comparison between the geometry of the ground and lowest excited state of the two conformers of **TPT**, computed at TD-CAM-B3LYP/6-31G* in vacuo.

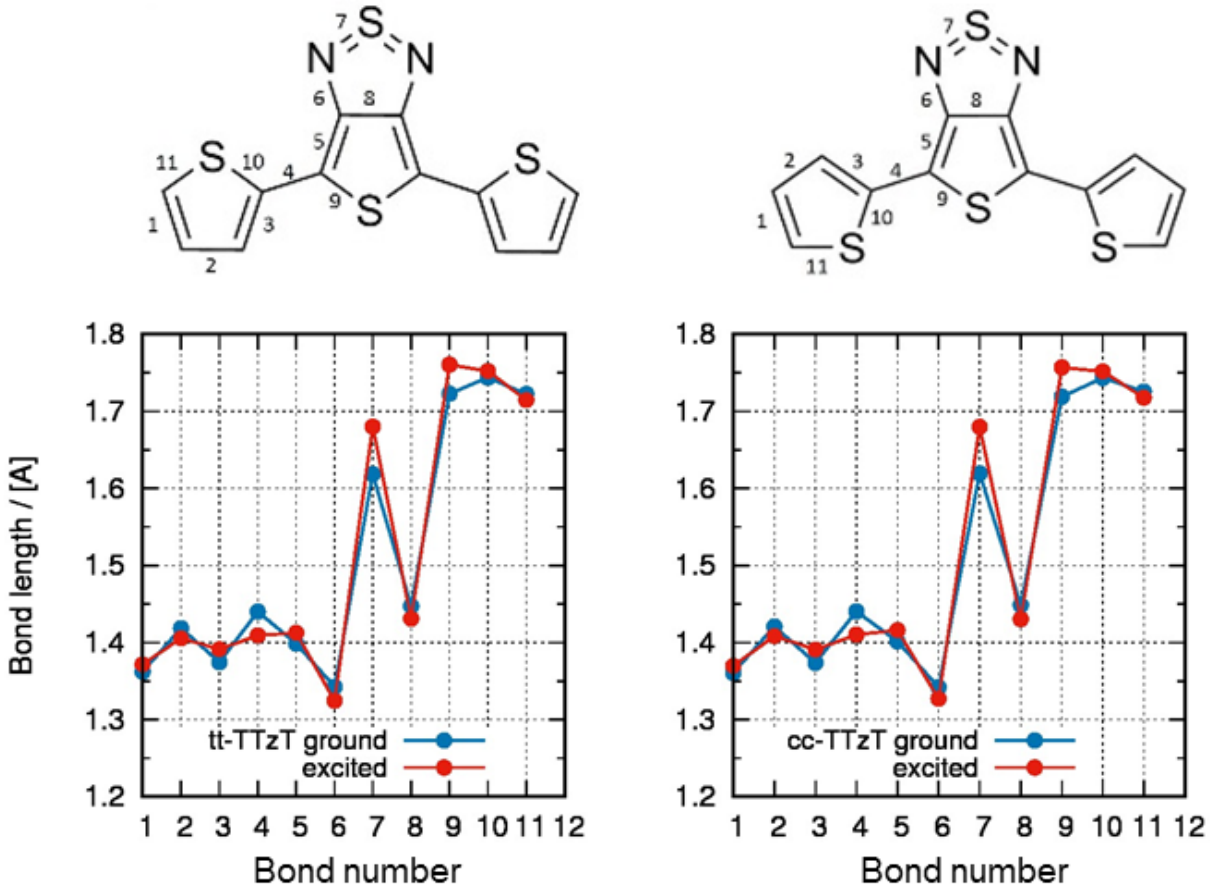

Figure S4. Comparison between the geometry of the ground and lowest excited state of the two conformers of **TTzT**, computed at TD-CAM-B3LYP/6-31G* in vacuo.

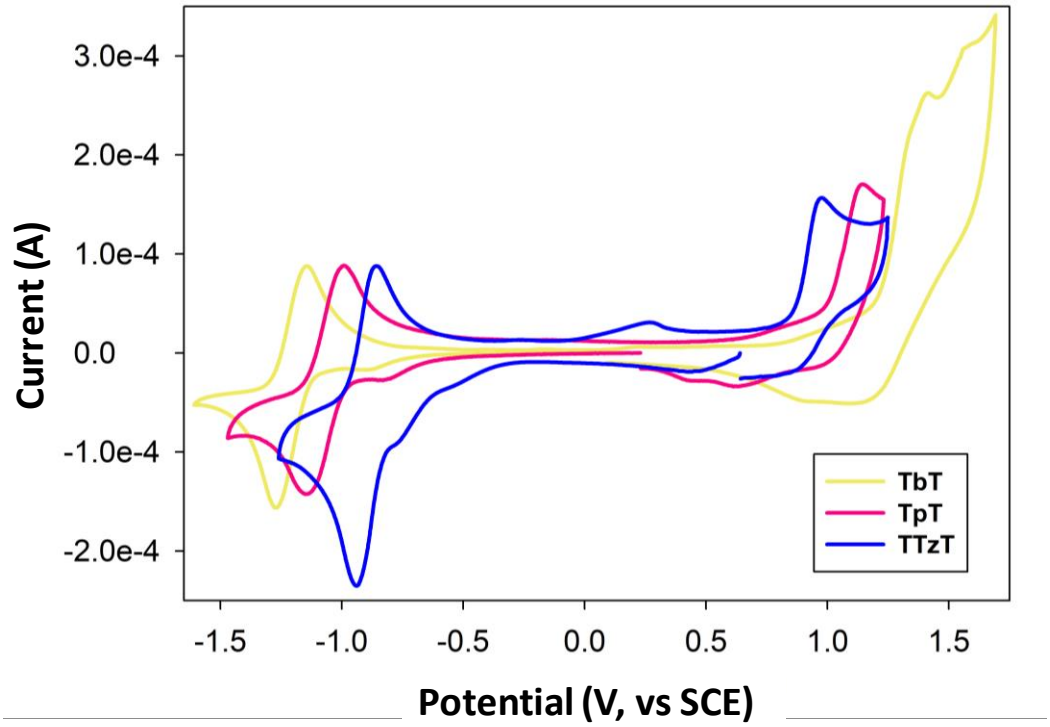

	ΔV (V)	ox (V, vs SCE)	red (V, vs SCE)
TbT	2.55	1.32	-1.23
TpT	2.21	1.14	-1.07
TTzT	1.95	1.04	-0.91

Figure S5. Cyclovoltammetry of **TBT** (yellow), **TPT** (red) and **TTzT** (blue) in CH_2Cl_2 with $TBAPF_6$ as electrolyte. Scan speed 0.1 V/s.

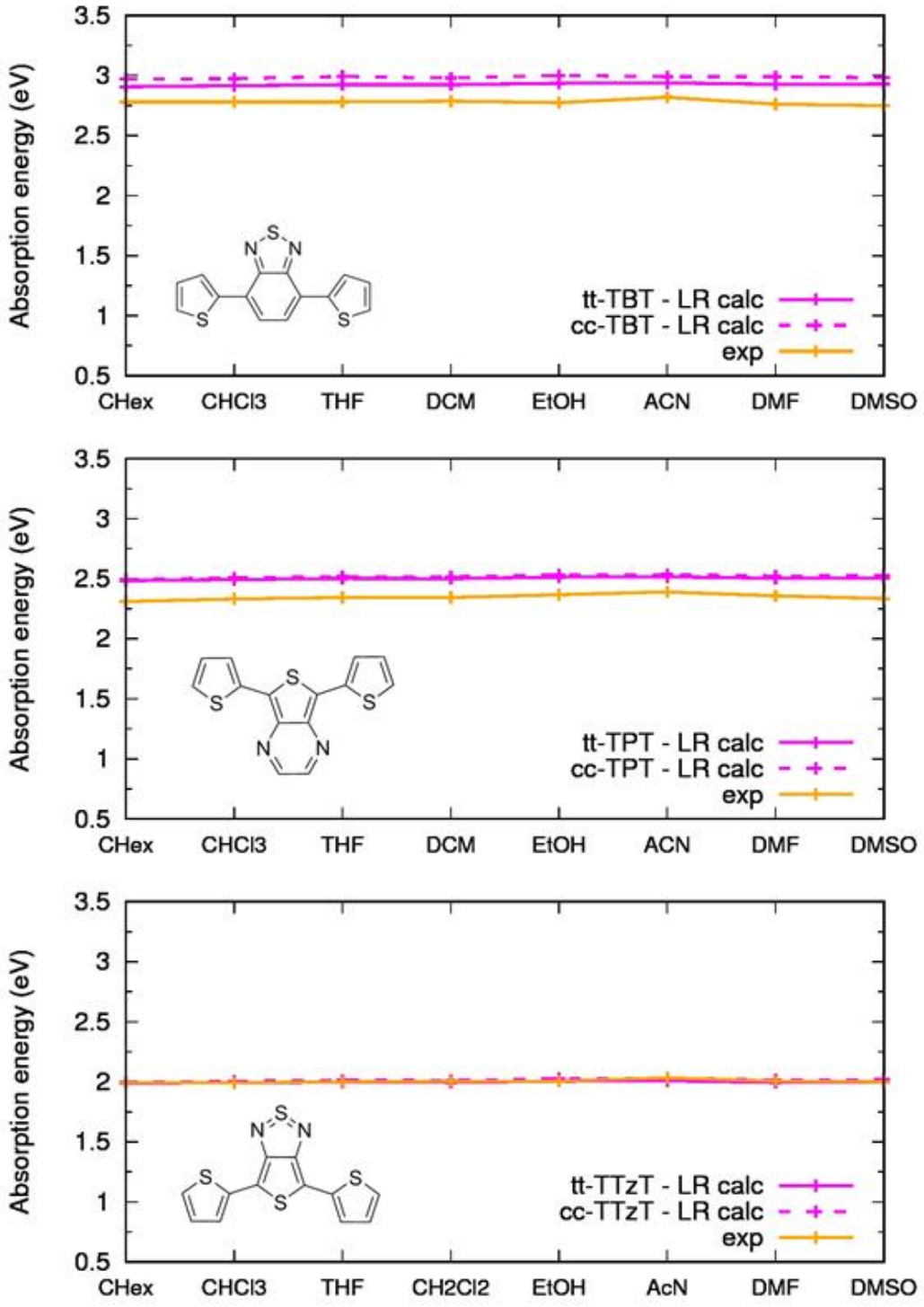

Figure S6. Comparison between experimental and computed absorption energies for the lowest energy absorption band, from TD-CAM-B3LYP/6-31G* vertical excitation energy calculations. Solvent described with the PCM method.

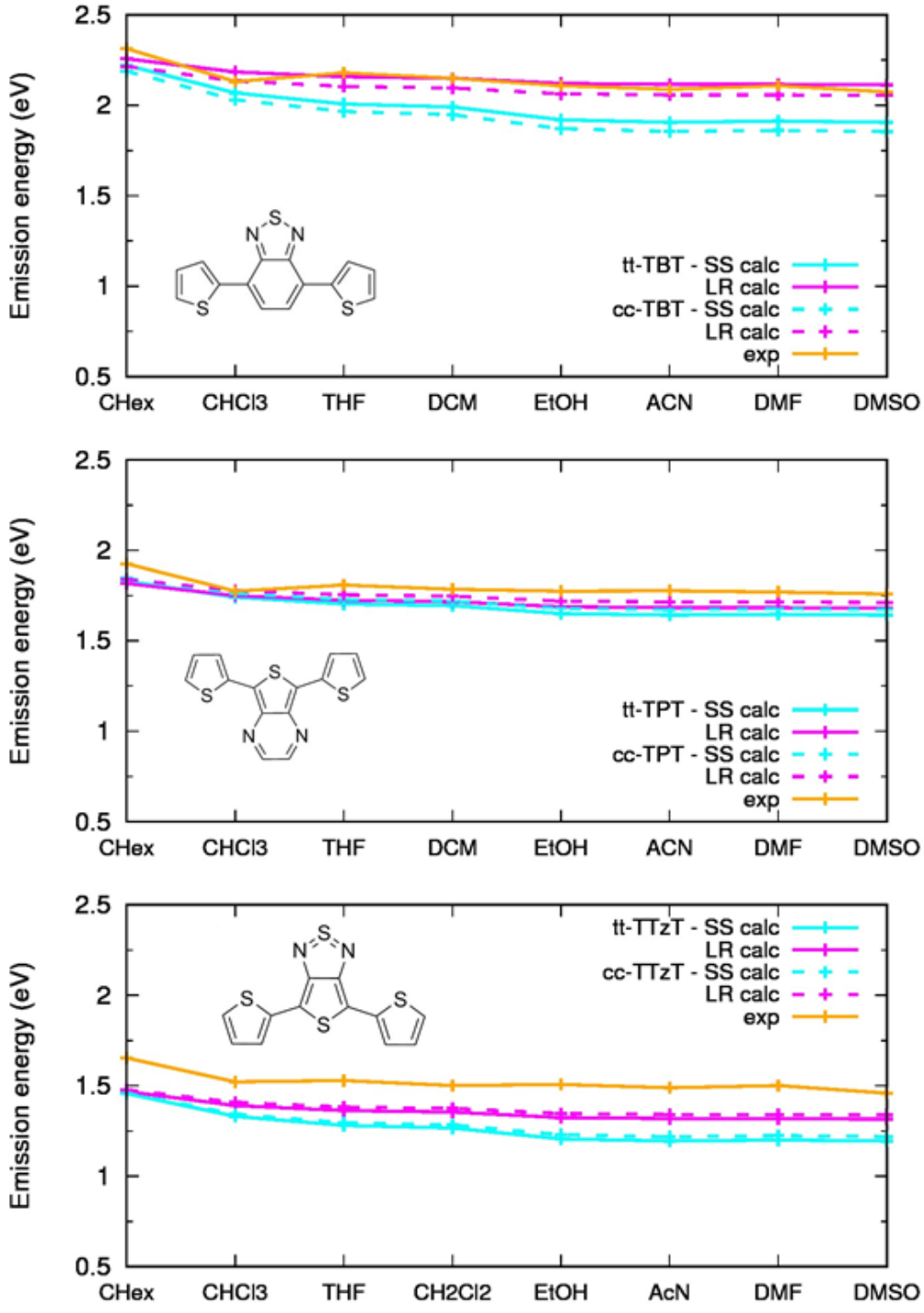

Figure S7. Comparison between experimental and computed emission energies from TD-CAM-B3LYP/6-31G* calculations at the geometry of the lowest excited state determined with the LR approach. Vertical emission energies computed with Linear Response (LR-PCM) and State Specific (SS-PCM) approaches.

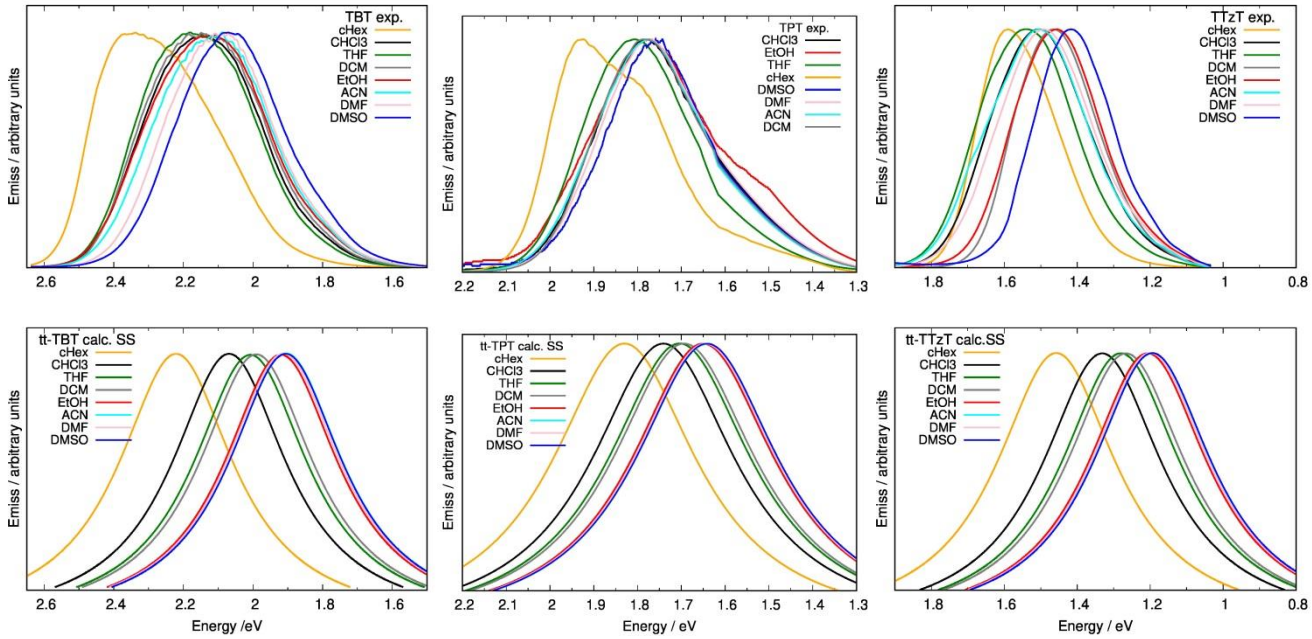

Figure S8. Comparison between experimental and computed emission energies from TD-CAM-B3LYP/6-31G* calculations at the geometry of the lowest excited state determined with the LR approach. Vertical emission energies computed with the State Specific (SS-PCM) method. These figures correspond to those shown in Figs. 4-6 right except that here emission energy is in eV.

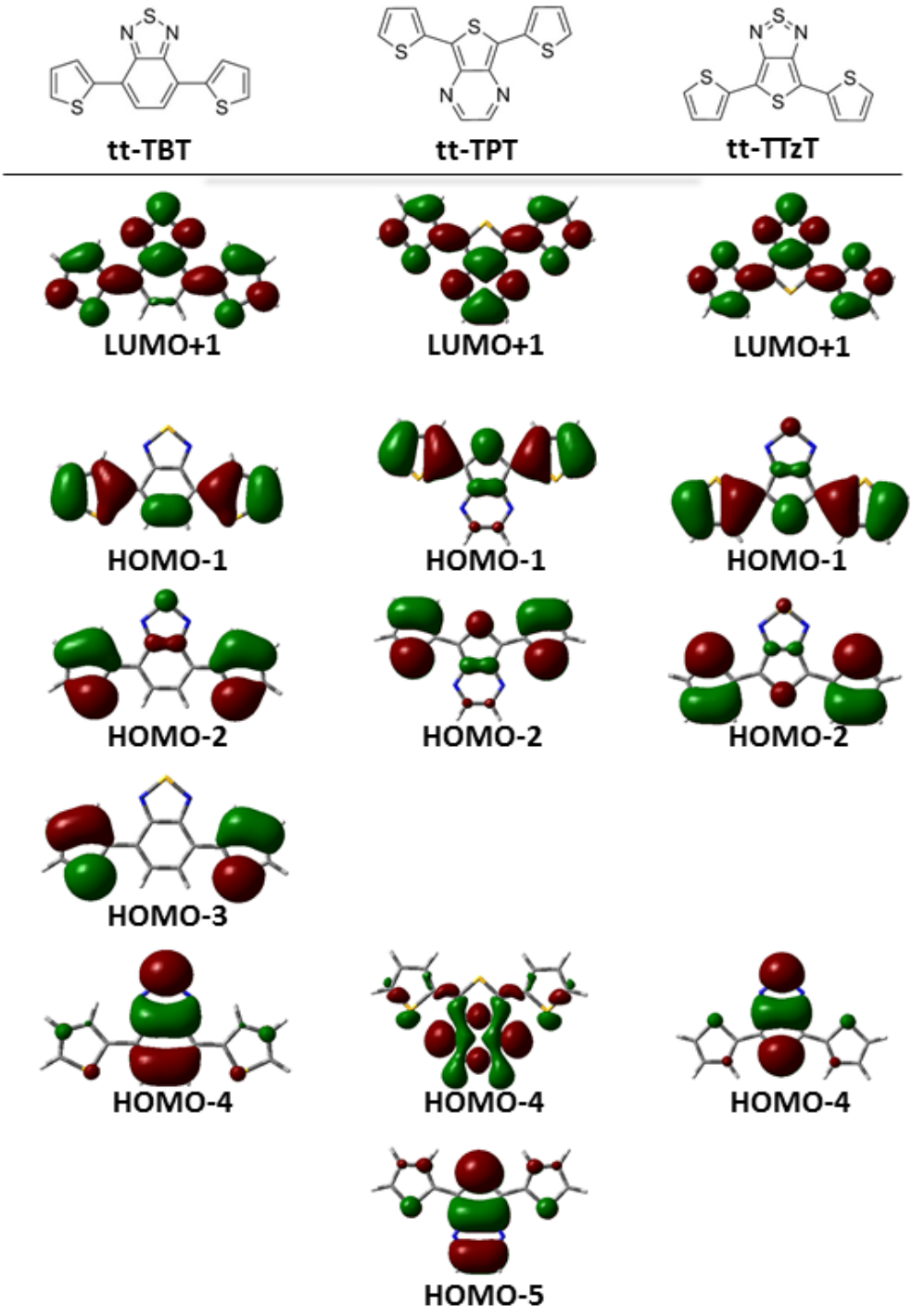

Figure S9. Molecular orbitals of **TBT, TPT** and **TTzT** relevant for the analysis of the lowest excited states from TD-CAM-B3LYP/6-31G* calculations.

Experimental apparatus for two-photon absorption spectroscopy

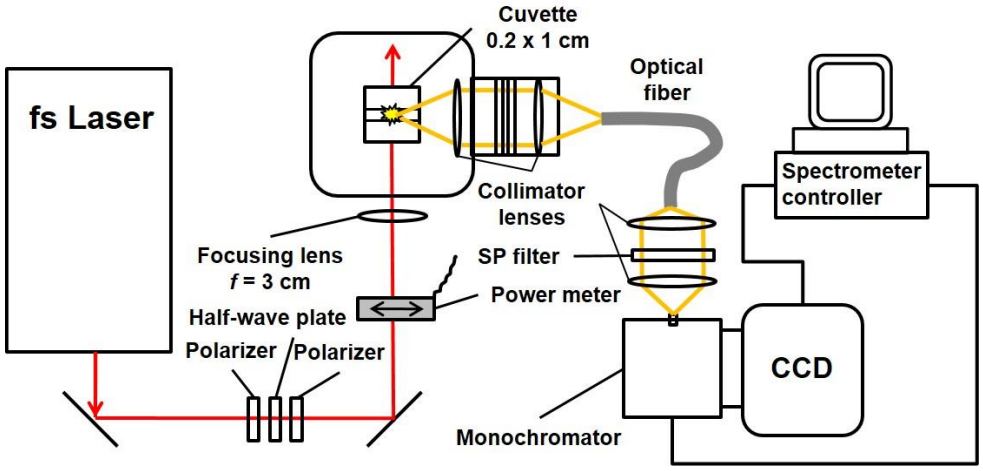

Fig. S10. Experimental apparatus for two-photon spectroscopy

The system for 2PA measurements employed in this work was based on a previously described setup [18].

The output of a tunable Ti:Sapphire laser (Chameleon Ultra II, Coherent; 80 MHz rep. rate) was passed through a half-wave plate and a polarizer for power adjustment and focused by a lens (f=3 cm) in the center of a cuvette (2 mm optical path) containing the sample solution. An optical power meter (FieldMaxII-TOP, Coherent) was used to measure the incident power immediately before the cell.

The emission was collected by a convex lens (2.5 cm diameter) placed next to the cell compartment at 90^{o} relative to the direction of the excitation beam and focused by another lens onto a glass fiber. At the other hand of the fiber, the light was collimated by a lens and focused onto the aperture of a monochromator. Short-pass filters were used to prevent the excitation light from reaching the detector.

The emission spectrum dispersed by the monochromator was imaged by a CCD camera (Andor iStar ICCD DH334T-18F-73). The measured signals were corrected to remove the effect of the instrument-response function (see below).

The average excitation power of ca. 50 mW was used in the experiments, i.e. well below the saturation threshold, when the plot of the emission intensity vs power started deviating from being strictly quadratic.

Deuterated solvents were used in all measurements in order to avoid absorption of the excitation light by C-H vibrational overtones [19], which may interfere with 2PA measurements.

Calculation of two-photon absorption cross-sections

The signals of the solution of a sample and of the reference (Rhodamine B in MeOD), both with known 1P absorbance, were recorded under 1P excitation by a LED (λ_{max} = 523 nm, Ledengin) in the same optical configuration as used in 2PA measurements. The relative sensitivities (R_{RS} reference/sample) of the setup were then calculated by normalizing the measured emission signals by the relative numbers of the absorbed photons, calculated by integrating the overlap between the absorption spectrum of the solution and the emission spectrum of the LED. The latter was measured using a FS920 spectrofluorometer (Edinburgh Instruments. UK), calibrated using a lamp with NIST-traceable spectral radiant flux (RS-15-50, Gamma Scientific, SN HL1956). Thus determined relative sensitivities R_{RS} included the effects of different quantum yields, solvent refractive indexes and detection efficiencies with respect to the different emission spectra.

The overall formula used for the calculation of 2PA cross-sections was:

$$\sigma_S^{(2)} = \sigma_R^{(2)} \cdot \frac{I_S}{I_R} \cdot \frac{\Phi_S^2}{\Phi_R^2} \cdot \frac{c_S}{c_R} \cdot R_{RS},$$

where $\sigma^{(2)}$ is the 2PA cross-section, I is the measured emission intensity, Φ is the excitation photon flux, c is concentration as calculated from the absorption spectra, and indexes S and R refer to the *sample* and *reference*, respectively. The instantaneous excitation flux Φ was calculated assuming a rectangular pulse of the duration equal to the FWHM of the actual pulse for each wavelength, as disclosed by the vendor (Coherent).

680 nm

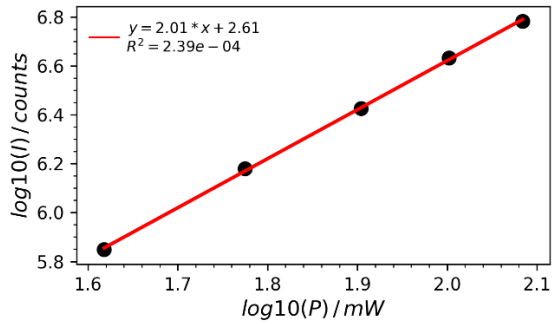

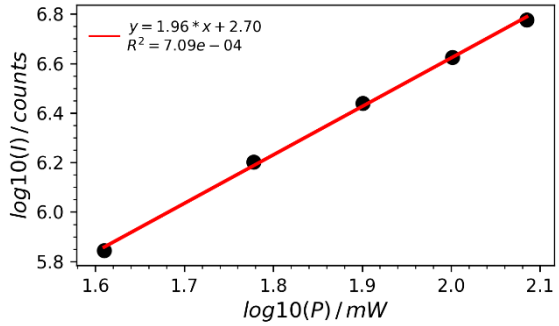

800 nm

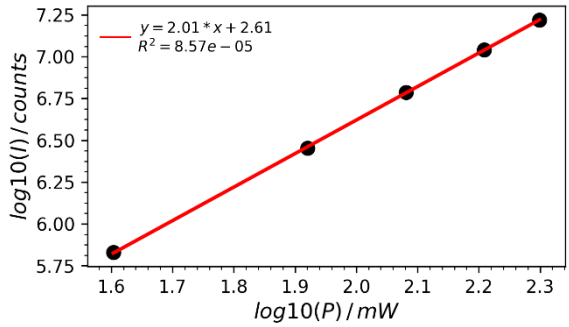

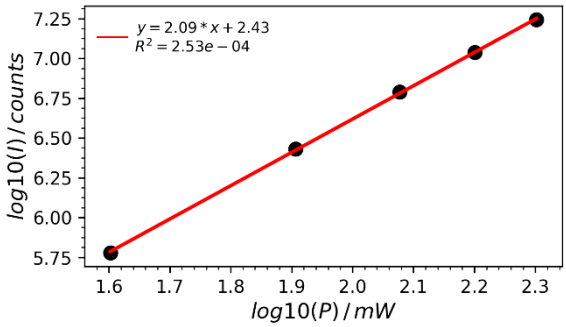

900 nm

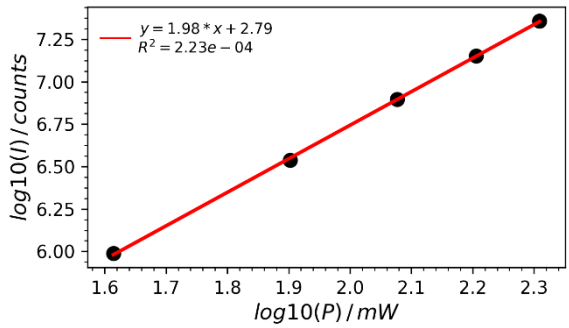

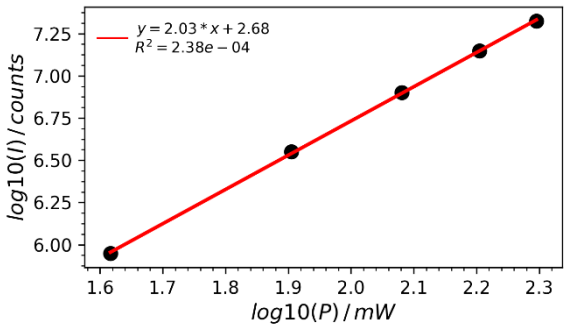

Figure S11. Power dependencies for **TBT** at different wavelengths.

740 nm

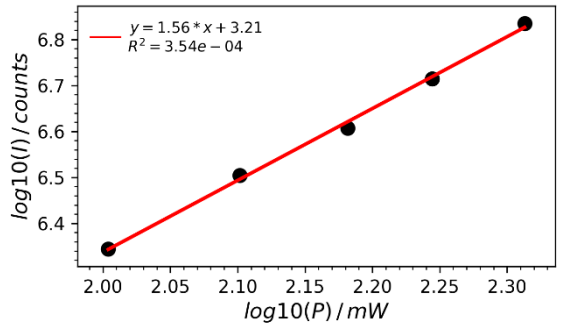

750 nm

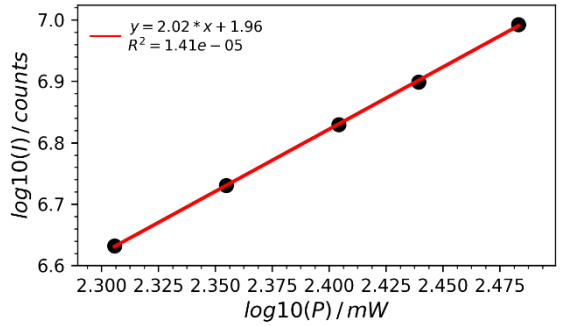

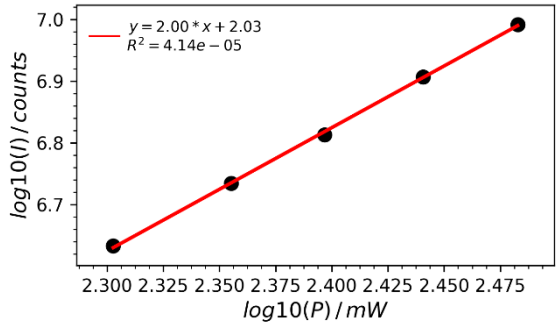

800 nm

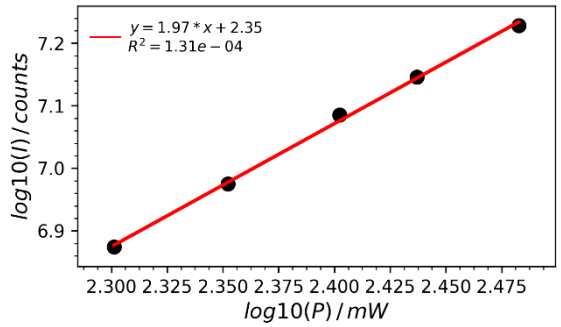

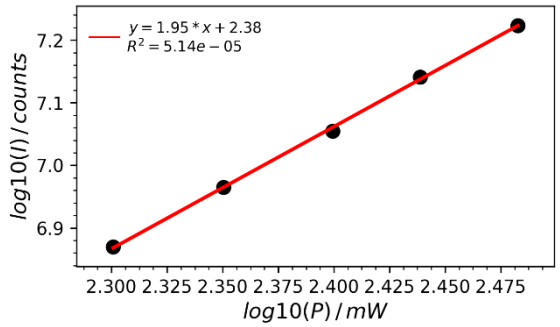

Figure S12. Power dependencies for **TPT** at different wavelengths.

1020 nm

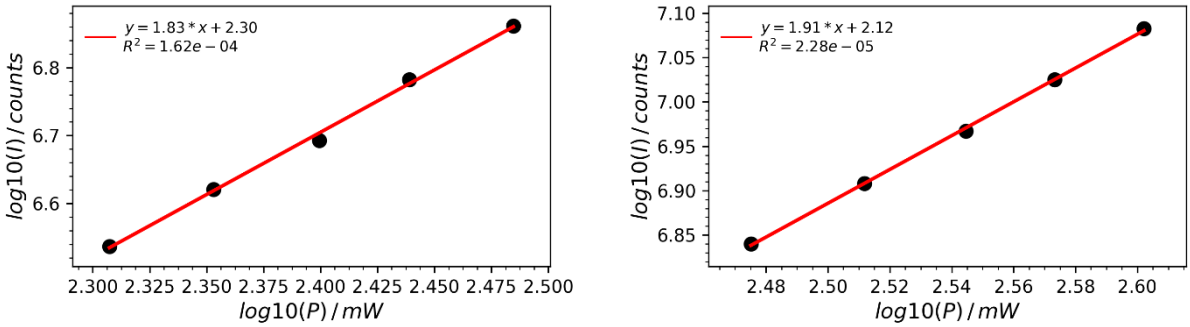

Figure S12. Continued - Power dependencies for **TPT** at different wavelengths.

930 nm

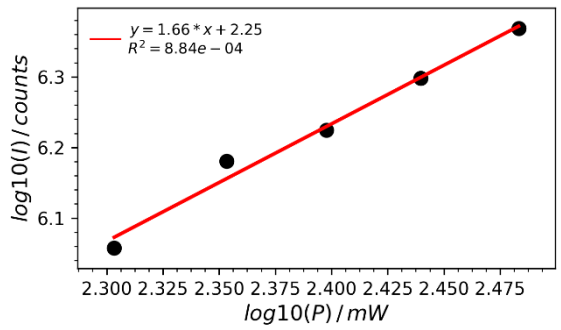

940 nm

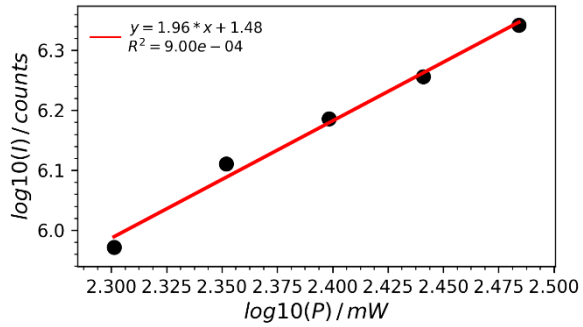

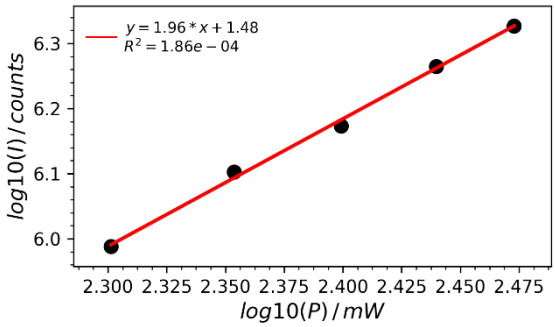

960 nm

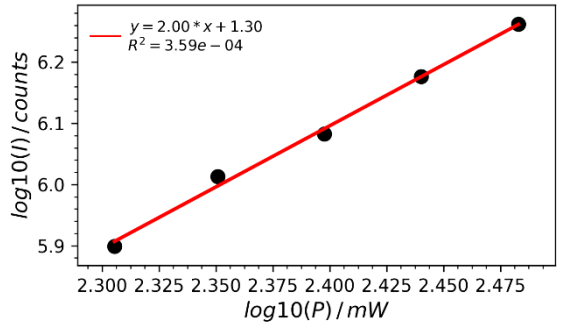

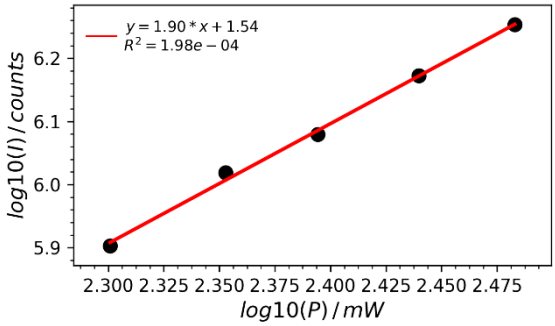

Figure S13. Power dependencies for **TTzT** at different wavelengths.

1000 nm

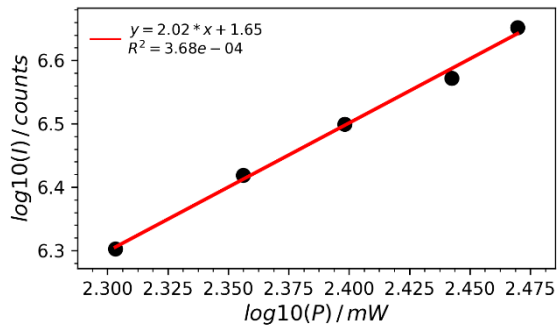

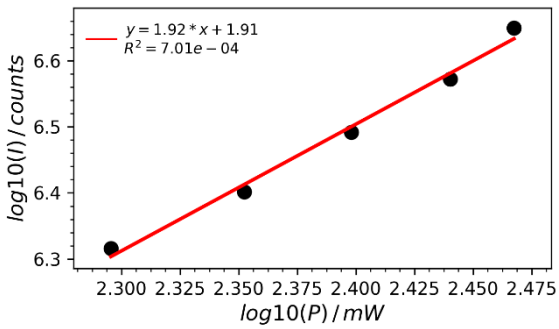

1080 nm

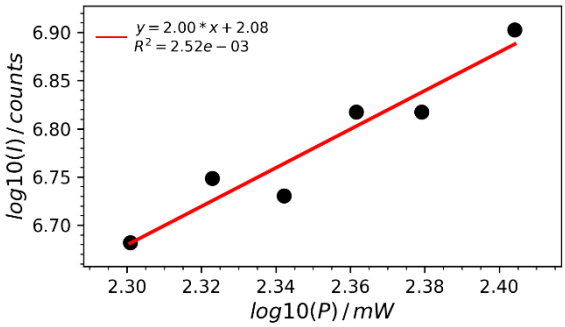

Figure S13. Continued - Power dependencies for **TTzT** at different wavelengths.

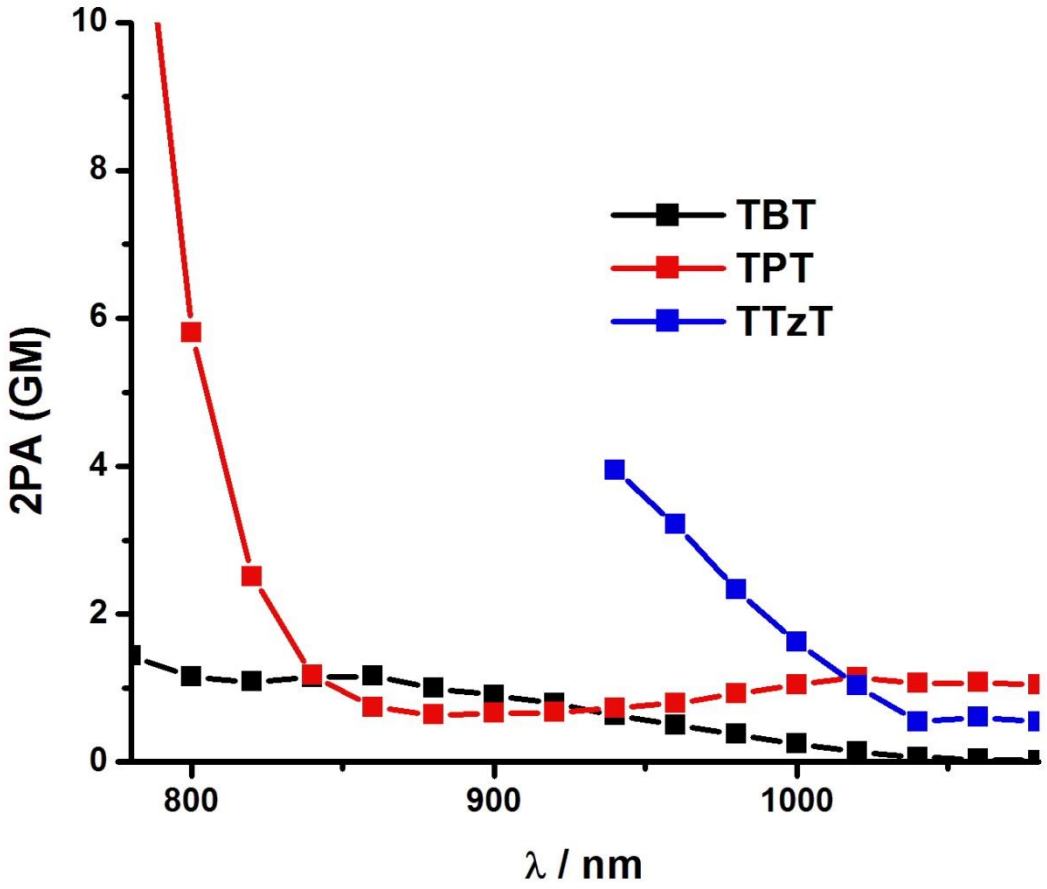

Figure S14. 2P absorption of **TBT**, **TPT** and **TTzT** in CDCl3 showing, in agreement with computed results (see Table S6) the weak cross-section in the region of the S_0-S_1 transition of **TBT** and **TPT**.

References

[1] F. Negri and G. Orlandi, *J. Chem. Phys.*, 1995, **103**, 2412-2419.
[2] F. Negri and M. Z. Zgierski, *J. Chem. Phys.*, 1995, **102**, 5165-5173.
[3] F. Negri and G. Orlandi in Computational Photochemistry, M. Olivucci Ed., Elsevier, 2005, 129-169.
[4] J.-L. Bredas, D. Beljonne, V. Coropceanu and J. Cornil, *Chem. Rev.*, 2004, **104**, 4971-5003.
[5] V. Coropceanu, J. Cornil, D. A. da Silva, Y. Olivier, R. Silbey and J.-L. Bredas, *Chem. Rev.*, 2007, *107*, 926-952.
[6] F. Duschinsky, *Acta Physicochim. URSS*, 1937, **7**, 551.
[7] M. Dierksen and S. Grimme, *J. Chem. Phys.*, 2004, **120**, 3544-3554.
[8] F. Santoro, A. Lami, R. Improta, J. Bloino and V. Barone, *J. Chem. Phys.*, 2008, **128**, 224311.
[9] H. C. Jankowiak, J. L. Stuber and R. Berger, *J. Chem. Phys.*, 2007, **127**, 234101.
[10] F. Santoro, R. Improta, A. Lami, J. Bloino and V. Barone, *J. Chem. Phys.*, 2007, **126**, 084509.
[11] F. Santoro, A. Lami, R. Improta and V. Barone, *J. Chem. Phys.*, 2007, **126**, 184102.
[12] M. Dierksen and S. Grimme, *J. Chem. Phys.*, 2005, **122**, 244101.
[13] R. Borrelli and A. Peluso, *J. Chem. Phys.*, 2003, **119**, 8437-8448.
[14] V. Barone, J. Bloino, M. Biczysko and F. Santoro, *J. Chem. Theory Comput.*, 2009, **5**, 540-554.
[15] S. Grimme in *Reviews in Computational Chemistry, Vol 20*, Ed. 2004, Vol. p 153-218.
[16] M. Malagoli, V. Coropceanu, D. A. da Silva Filho and J.-L. Brèdas, *J. Chem. Phys.*, 2004, **120**, 7490-7496.
[17] C. J. Ballhausen "Molecular electronic structures of transition Metal Complexes", Mc.Graw-Hill, New York, 1979.
[18] T. V. Esipova, H. J. Rivera-Jacquez, B. Weber, A. E. Masunov, S. A. Vinogradov, *J. Am. Chem. Soc.* 2016, 138, 15648-15662
[19] M. Plidschun, M. Chemnitz and M. A. Schmidt, *Optical Materials Express,* 2017, **7**, 1122-1130.